ISSN 0036-0236, Russian Journal of Inorganic Chemistry, 2021, Vol. 66, No. 5, pp. 747–754. © Pleiades Publishing, Ltd., 2021.
Russian Text © The Author(s), 2021, published in Zhurnal Neorganicheskoi Khimii, 2021, Vol. 66, No. 5, pp. 648–657.

INORGANIC MATERIALS AND NANOMATERIALS

Dependence of the Reactivity of the Finely Divided System Ta_2O_5–HfO_2–C on the Xerogel Carbonization Temperature

E. P. Simonenko[a, *], N. P. Simonenko[a], I. A. Nagornov[a, b], A. S. Mokrushin[a], M. V. Maltseva[a, b], V. G. Sevastyanov[a], and N. T. Kuznetsov[a]

[a] *Kurnakov Institute of General and Inorganic Chemistry, Russian Academy of Sciences, Moscow, 119991 Russia*
[b] *Mendeleev University of Chemical Technology of Russia, Moscow, 125047 Russia*
**e-mail: ep_simonenko@mail.ru*

Received December 14, 2020; revised December 22, 2020; accepted December 23, 2020

Abstract—The effect of the temperature of carbonization of xerogels on the chemical activity of the obtained materials in the Ta_2O_5–HfO_2–C system was studied to create an energy-efficient method for producing ceramic materials based on the TaC–HfC system using reactive hot pressing or spark plasma sintering. A new method was developed to form a tantalum–hafnium–polymer-containing gel by creating interpenetrating organic–inorganic networks with the simultaneous initiation of hydrolysis of metal–containing precursors and polymerization of furfuryl alcohol (acid catalysis with formic acid). Samples of the Ta_2O_5–HfO_2–C system with different reactivities in the carbothermal synthesis of complex carbides were obtained based on the xerogel produced after drying using carbonization under dynamic vacuum conditions at various temperatures (400, 700, and 1000°C). Their elemental and phase composition, microstructure and thermal behavior in an air flow were investigated. The powder synthesized at a minimum temperature of 400°C had the maximum reactivity but also contained rather much (3–4 wt %) unpyrolyzed organic fragments, which should be taken into account in planning high-temperature consolidation of carbide ceramics.

Keywords: sol–gel technology, ultrarefractory carbide, nanopowder, carbothermic reduction
DOI: 10.1134/S003602362105020X

INTRODUCTION

Since the 1930s–1960s [1–8], ultrarefractory carbides of 4B and 5B group elements have attracted close attention by their unique properties. Among them are not only high melting points in the range 2800–4000°C, but also high hardness, high strength, low vapor pressure at very high temperatures [5, 9], interesting magnetic properties, and also relatively high electrical and thermal conductivity. Moreover, it is known that cubic monocarbides of these elements owing to their isostructurality form a continuous series of solid solutions [10–14], which allows one to finely tune necessary characteristics.

Of greatest interest is the TaC–HfC system, because it is in this system that there is a material, 4TaC–1HfC (Ta_4HfC_5), that has the highest melting point (~4000°C) of the currently existing materials [4, 6]. Recent design solutions in the aerospace industry have led to an abrupt increase in the demand in such ultrarefractory compounds, which stimulated new studies aimed at precisely determining the melting point of this material. For example, Cedillos-Barraza et al. determined by laser heating [15] that the melting point of this material is somewhat lower than that of individual hafnium carbide. This conclusion was refuted by Savvatimskiy et al. [16], who, using rapid heating by a microsecond electric current pulse, confirmed that the melting point of Ta_4HfC_5 is about 4300 ± 80 K, which is noticeably higher than the melting points of HfC and TaC.

Studies of the fundamental properties of ultrarefractory carbides were resumed with a view to their potential use for producing ultra-high-temperature carbide ceramic materials [17–20], and also for doping ceramic materials based on the MB_2–SiC systems (M = Zr, Hf) [21–27]. For example, we previously showed that the addition of 10 vol % of finely divided complex carbide Ta_4HfC_5 increases the oxidation resistance of the HfB_2–30 vol % SiC ceramic on long-term exposure to a supersonic dissociated air flow [23].

Reactive hot pressing or spark plasma sintering of oxygen-free ceramics has significant advantages over consolidation of mixtures of powders of refractory phases [28–31]; in particular, it can be performed at relatively low sintering temperatures and gives ceramics with the minimum grain size, which improves their mechanical and thermal properties. Moreover, the formed carbide phases are often nanocrystalline [24]. To efficiently use this method, the initial systems should have the maximum reactivity and the maxi-

mum uniform mutual distribution of oxide and carbon components.

In our previous works [29, 32–35], the controlled hydrolysis of metal-containing precursors (alkoxides and alkoxoacetylacetonates of metals) in a solution of phenol formaldehyde resin was used. The pyrolysis of this resin in the course of the carbonization in a medium of an inert gas or in a dynamic vacuum gave amorphous carbon, which was necessary for the relatively low-temperature synthesis of refractory carbides. This procedure has certain advantages, but depending on the type of precursor, the components may sometimes salt out each other, which leads to phase separation of the system and to a less uniform distribution of the constituents of the MO_x–C material formed after the carbonization.

Approaches have recently been developed to obtain finely divided refractory carbides (primarily as aerogels) by the formation of the so-termed interpenetrating organic–inorganic networks [36–43]. To form a connected-disperse system, which can inherit a virtually homogeneous distribution of the oxide components and the polymer from the stage of solutions, several processes are simultaneously started, namely, hydrolysis of precursors with subsequent polycondensation (the first three-dimensional network) and polymerization of the monomer, which forms the second three-dimensional network. Such studies typically concern the synthesis of nanocrystalline silicon carbide with high specific surface area by the hydrolysis of tetraethoxysilane and the polymerization of resorcin with formaldehyde [40–43] or furfuryl alcohol [44–46]. Nanopowders or porous ceramics were also synthesized based on titanium carbides [47–50] and zirconium [51, 52], but we failed to find any studies of the possibility of the synthesis of element 5B group carbides or mixed carbides by the described method.

The purpose of this work is to characterize the dependence between the reactivity of the finely divided system Ta_2O_5–HfO_2–C in the carbothermal synthesis of tantalum hafnium carbide 9TaC–1HfC and the carbonization temperature of the tantalum–hafnium–polymer-containing xerogel obtained by the simultaneous polymerization of the products of the hydrolysis of metal-containing precursors and furfuryl alcohol.

EXPERIMENTAL

Hafnium alkoxoacetylacetonate was synthesized by the heat treatment of a solution of hafnium acetylacetonate (>99%) in isoamyl alcohol (>98%, EKOS-1) at an oil bath temperature of 150–160°C for 6 h [33, 53]. A solution of tantalum pentabutoxide was prepared by the interaction of tantalum pentachloride (99.995%, Lanhit) with *n*-butanol (>98%, Khimmed) while bubbling with dried ammonia with subsequent separation of the precipitate by centrifugation at 3500 rpm for 30 min.

To obtain a tantalum–hafnium–polymer-containing gel, an aliquot of the hafnium halkoxoacetylacetonate solution was added to the solution of tantalum pentabutoxide $Ta(OBu)_5$ so that the $n(Ta) : n(Hf)$ ratio was 9 : 1. Then, the obtained mixture was supplemented while stirring with furfuryl alcohol $C_5H_6O_2$ (98%, Acros Organics) to an $n(C_5H_6O_2) : n(Ta + Hf)$ ratio of 1.5, with formic acid CH_2O_2 (>98%, Spektr-Khim) as a catalyst of polymerization of furfuryl alcohol ($n(CH_2O_2) : n(Ta + Hf) = 4.5$), and with a hydrolyzing mixture (a 10 vol % solution of distilled water in ethanol). The amount of water in the solution corresponded to the ratio $n(H_2O) : n(Ta + Hf) = 10$. After the mixing of all the components, a transparent solution was obtained (Fig. 1a), which transformed into a dense gel in ~2 min after the beginning of heating on a water bath with a temperature of 90–95°C. Simultaneously, as is seen from Fig. 1a, the system darkened, which suggested that furfuryl alcohol was being polymerized. In 20–25 min after the beginning of the heating, a dense dark brown gel formed, which was further dried at 110–120°C until the weight ceased to change.

The thermal behavior of the obtained finely divided powders in the Ta_2O_5–HfO_2–C system was studied with an SDT Q-600 simultaneous TGA/DSC/DTA analyzer in the temperature range 20–1400°C (heating rate 20 deg/min) in a flow of either air or argon (flow rate 250 mL/min).

The X-ray powder diffraction patterns of the produced powders in the initial system Ta_2O_5–HfO_2–C and the products of their reduction were recorded with a Bruker D8 ADVANCE X-ray powder diffractometer (CuK_α radiation, resolution 0.02°, signal integration time at point 0.3 s). The X-ray powder diffraction data were analyzed using Match!—Phase Identification from Powder Diffraction, Version 3.8.0.137 (Crystal Impact, Germany), into which the Crystallography Open Database (COD) is embedded.

The scanning electron microscopy of intermediate nanocomposites and products was carried out with a Carl Zeiss NVision 40 focused ion beam scanning electron microscope. The elemental composition was estimated in regions 2 × 3 mm in size using an Oxford Instruments energy-dispersive X-ray analyzer.

RESULTS AND DISCUSSION

The thermal analysis of the obtained xerogel in an argon flow (Fig. 1b) suggested that the pyrolysis of its organic fragments occurs in several steps. Up to approximately 250–270°C, the weight loss is due to the evaporation of volatile components, which is represented by the intense endothermic effect with a minimum at ~175°C and arms at 90 and 250°C. A further increase in temperature initiates the thermal decom-

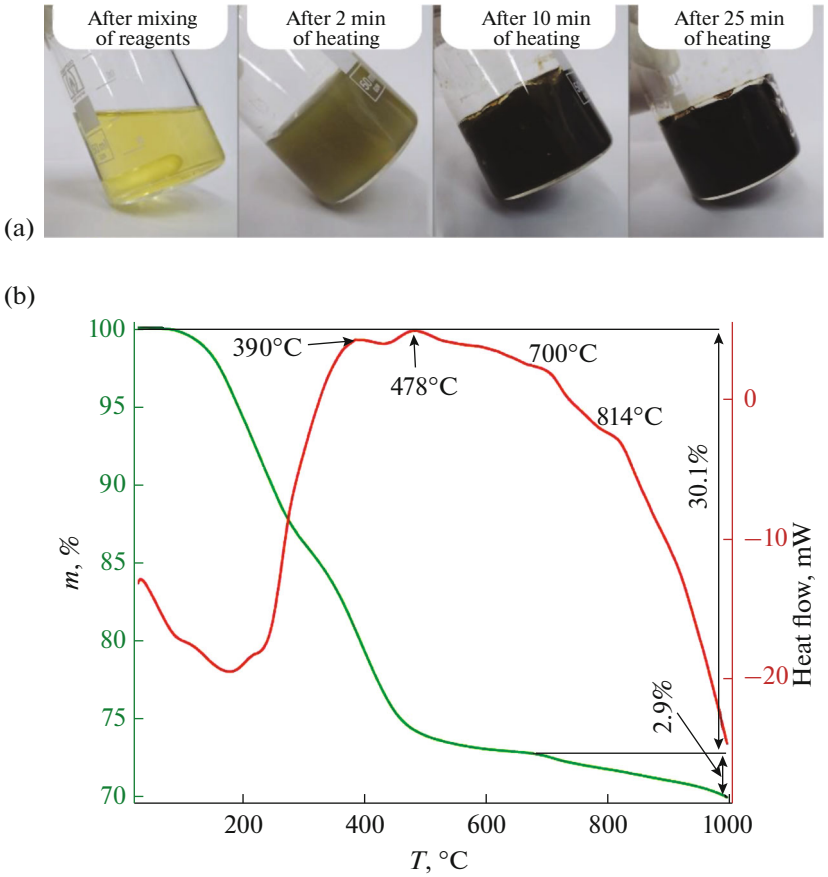

Fig. 1. Views of the tantalum–hafnium–polymer-containing system at different times of gel production, and (b) the DSC (red) and TGA (green) curves of the thermal analysis of the xerogel in an argon flow.

position of organic fragments, which is characterized by the broadened weak exothermic effect with maxima at 390, 478, 700, and 814°C.

As Fig. 1b shows, the weight loss is maximum at temperatures <400–500°C and is 21–26%. The total weight loss due to the carbonization of the xerogel in an argon flow during heating to 700°C is 30%, and further heating to 1000°C leads to an increase in Δm to 33%. The change in the slope of the TGA curve at ~700°C can be caused both by the domination of the dehydrogenation of aromatic fragments, and by the beginning of the carbothermal synthesis of complex tantalum hafnium carbides.

Based on the DSC/TGA data, the carbonization temperatures 400, 700, and 1000°C were chosen to estimate the reactivity of the Ta_2O_5–HfO_2–C materials. The pyrolysis of organic fragments of the xerogels was performed in graphite boats under dynamic vacuum conditions (residual pressure 30–100 Pa). The heating rates were 400 and 200 deg/h in the temperature ranges 20–700 and 700–1000°C, respectively; the time of holding at a given temperature was 2 h.

The scanning electron microscopy showed (Fig. 2) that the microstructure of the produced Ta_2O_5–HfO_2–C materials, regardless of the xerogel carbonization temperature, somewhat differs from that observed for such systems obtained using phenol formaldehyde resin [33, 35, 54]. The powders are obviously less porous, and the approximate particle size with increasing heat-treatment temperature from 400 to 1000°C decreases from 50–60 to 20–30 nm. Such a dense morphology may be due to the fact that, at the gelation step, two polymer networks simultaneously formed, which, during shrinkage, more rigidly fix the produced amorphous particles, probably, by forming mesoporous composites. The elemental energy-dispersive X-ray analysis both on area 2 × 3 mm and on area 2 × 3 mm showed that the ratio n(Ta) : n(Hf) is 89 : 11 with an error of ±1.2 for all the samples, which corresponds to the desired composition. At a carbonization temperature of 400°C, the sample contains an admixture of chlorine, probably, from the initial $TaCl_5$, which is absent at higher pyrolysis temperatures.

Figure 3 presents the X-ray powder diffraction patterns of the samples. The first pattern demonstrates that the dynamic heating of the xerogel to 1000°C at a rate of 20 deg/min in an argon flow leads to the crys-

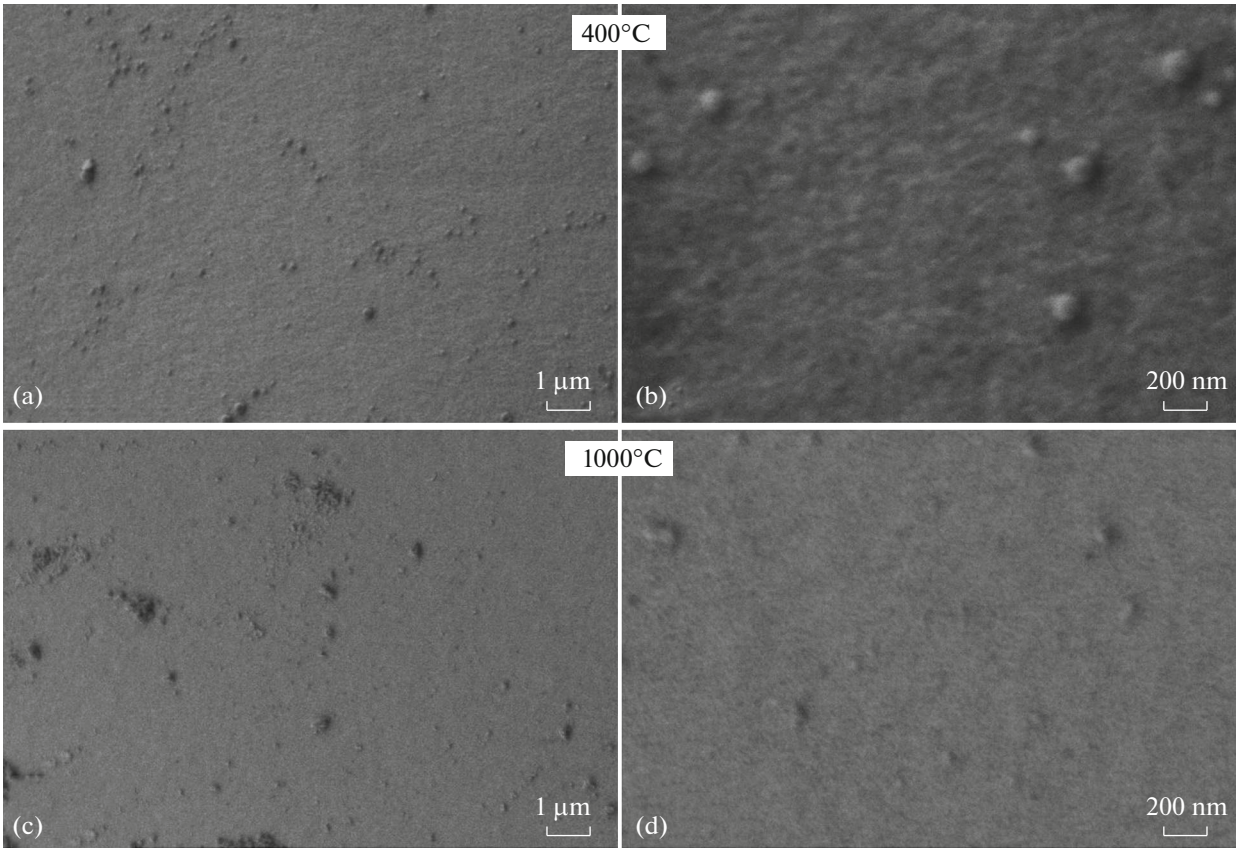

Fig. 2. Microstructure of the samples of the Ta_2O_5–HfO_2–C system that were obtained by the carbonization of the xerogels at (a, b) 400 and (c, d) 1000°C.

tallization of only orthorhombic Ta_2O_5 [55]. Longer carbonization of the xerogel (with holding for 2 h) at 400°C gives an X-ray amorphous substance (pattern *2*), which shows the signs of local structuring (diffuse halos). With an increase in the pyrolysis temperature to 700°C, the most intense reflections of the tantalum oxide phase also in the orthorhombic form begin to appear against the background of the halos (pattern *3*). In the sample subjected to the highest-temperature heating (carbonization at 1000°C), not only does the *o*-Ta_2O_5 phase forms [55], but also so does quite a large amount of a carbide phase based on TaC (pattern *4*). Obviously, the heat treatment under dynamic vacuum conditions at 1000°C initiates the carbothermal synthesis of (Ta,Hf)C, which, in the case of tantalum carbide, is not thermodynamically forbidden [33].

The thermal behavior in an air flow for the Ta_2O_5–HfO_2–C systems obtained at various temperatures was studied by simultaneous DSC/TGA (Fig. 4). It was determined that, in the samples obtained at 400 and 700°C, the weight loss is only due to the carbon burnout and, probably, underpyrolized organic fragments, first of all, aromatic. This process is represented by the broad and intense exothermic effect with a maximum at 560–580°C. Noteworthy, in the sample produced at 400°C, a significant weight loss begins at much lower temperatures (430–440°C), and the total weight loss Δm is maximum (–21.2%). Comparison with the weight loss (–17.8%) in the sample produced at 700°C suggests that the lowest-temperature sample contains organic fragments, which were incompletely transformed into amorphous carbon. Moreover, the DSC curve for the samples obtained at 400 and 700°C exhibits an exothermic effect that is unrelated to a weight change and is likely to correspond to the crystallization of Ta_2O_5.

At the same time, the thermal behavior of the sample obtained at a carbonization temperature of 1000°C differs considerably: at relatively low temperatures (>220–250°C), there is a weight gain by 2.6%, which is accompanied by the exothermic effect with a maximum at 393°C, probably, due to the oxidation of the carbide phase 9TaC–1HfC formed in the course of the carbonization. This thermal effect overlaps the next exothermic effect (with a maximum at 580°C) related to the oxidation of carbon in the initial system. The observed weight loss is only 9.8%, which also confirms the above conclusion on the partially completed carbothermal synthesis directly in the process of the pyrolysis of organic components at 1000°C. The content of the carbide phase in the initial powder was esti-

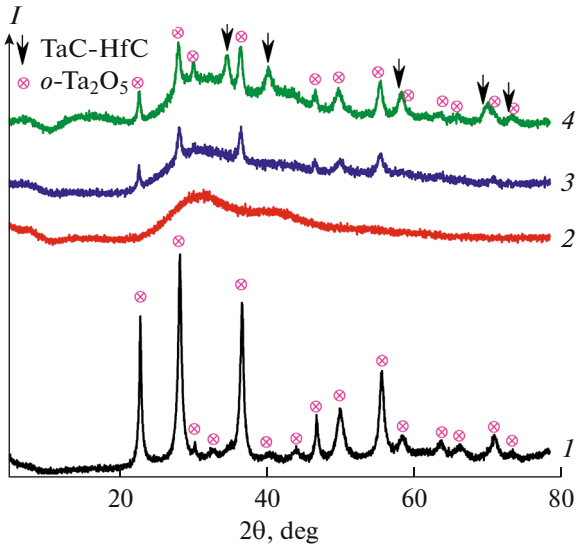

Fig. 3. X-ray powder diffraction patterns of the samples obtained by (*1*) the thermal analysis of the xerogel in an argon flow and the carbonization of xerogels at (*2*) 400, (*3*) 700, and (*4*) 1000°C.

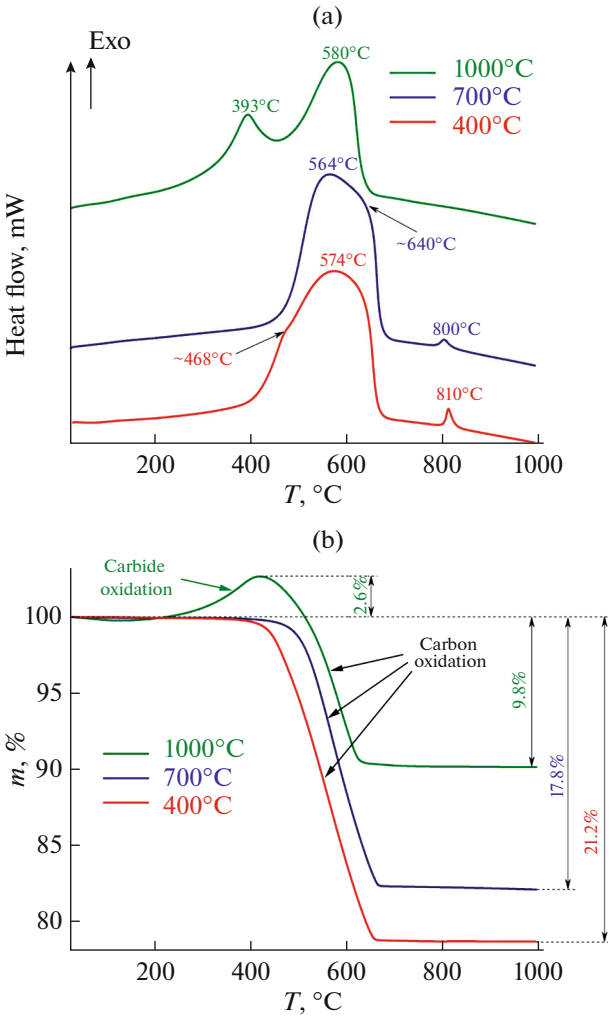

Fig. 4. Curves of (a) DSC and (b) TGA in an air flow for the samples obtained by the carbonization of the tantalum–hafnium–polymer-containing xerogels at 400, 700, and 1000°C.

mated under the assumption that the processes of the oxidation of the synthesized carbide and the pyrolytic carbon do not overlap, and that the weight gain 2.6% is due to the complete oxidation of TaC–HfC. The obtained results show that the system formed by the highest-temperature carbonization of the xerogel contains no less than 19–20 mol % carbide phase.

The reactivity of the produced samples in the carbothermal synthesis of tantalum hafnium carbide was estimated by studying their thermal behavior during heating in an argon flow to 1400°C (Fig. 5). For comparative experiments, weighed powder samples, 73 ± 5 mg each, were used.

It was shown that the weight loss is minimum (17.8%) in the sample of the initial system Ta_2O_5–HfO_2–C–(Ta,Hf)C obtained by the carbonization of the xerogel at the highest temperature 1000°C. This process is represented by the pronounced endothermic effect with a minimum at 1254°C.

Only a little higher (19.0%) weight loss due to the carbothermy is observed in the sample obtained at 700°C, and the DSC curve shows that the reaction process is stepwise: the thermal curve exhibits the broadened weak exothermic effect with a maximum at ~820°C, which is likely to be due to the thermal decomposition of residual organic fragments (weight loss ~1.3%). At higher temperatures, there are two endothermic effect with minima at 1094 and 1363°C, which gives the idea that carbides based on TaC and HfC can be synthesized separately. The hypothesis that the systems contain fractions with significantly different particle sizes and, hence, reactivities is unlikely because it is not confirmed by scanning electron microscopy data at various accelerating voltages.

The maximum (24%) weight loss due to the heating of the Ta_2O_5–HfO_2–C system to 1400°C in an argon flow is demonstrated by the sample produced at the minimum carbonization temperature 400°C. However, it should be taken into account that the measured weight change is a result of the following processes:

– the ultimate pyrolysis of organic fragments (characterized by the broadened and weak exothermic effect with maxima at 486, 742, and 802°C, the positions of which are close to those in the pyrolysis of the xerogel (Fig. 1b);

– the carbothermal synthesis of complex carbide (Ta,Hf)C, which is accompanied by the endothermic effect with maxima at 1104 and >1345°C.

The shift of the position of the first endothermic effect toward higher temperatures can be explained by

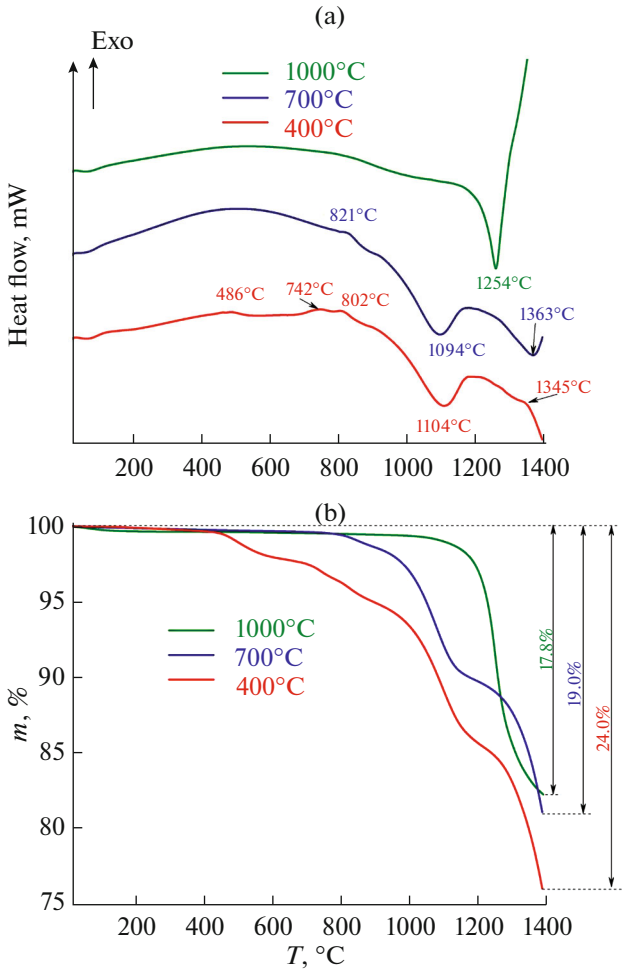

Fig. 5. Curves of (a) DSC and (b) TGA in an argon flow for the samples obtained by the carbonization of the tantalum–hafnium–polymer-containing xerogels at 400, 700, and 1000°C.

the partial overlap of the temperature ranges of the first and second processes. In the considered case, the two-phase system (Ta,Hf)C + (Hf,Ta)C with the definite domination of the first product can also form, which is, in principle, inherent in the low-temperature synthesis of tantalum hafnium carbides [35, 56, 57].

The X-ray powder diffraction patterns of the products obtained by heating the samples produced by the carbonization of the tantalum–hafnium–polymer-containing xerogels at various temperatures (400–1000°C) show the intense reflections corresponding to the phase of complex carbide (Ta,Hf)C based on tantalum carbide [58] with the unit cell parameter 4.451–4.453 Å, and also the reflections of the phase of orthorhombic tantalum oxide [55] (Fig. 6). The sample obtained at the highest temperature 1000°C, along with the above phases, also contains orthorhombic hafnium oxide [59] and the low-temperature form *o*-Ta_2O_5 [60].

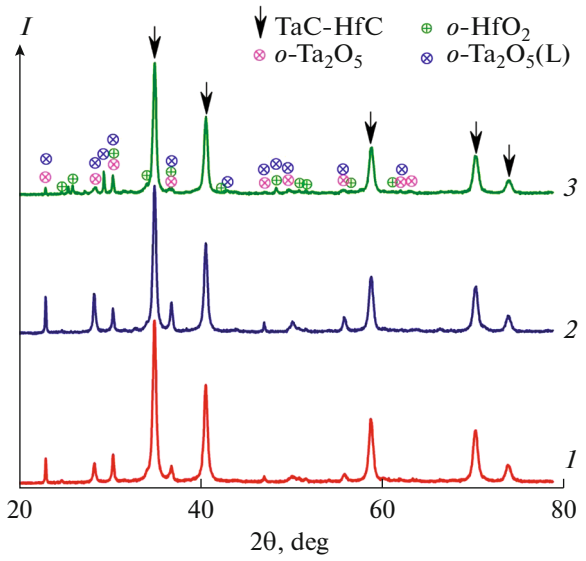

Fig. 6. X-ray powder diffraction patterns of the products of heating (to 1400°C, argon flow) of the samples obtained by the carbonization of the tantalum–hafnium–polymer-containing xerogels at (*1*) 400, (*2*) 700, and (*3*) 1000°C.

The estimation of the content of the phase (Ta,Hf)C in the obtained products by the Rietveld method demonstrated that its maximum amount (88.7%) formed by heating the sample synthesized at the minimum carbonization temperature 400°C, which is indicative of its high reactivity. The content of the carbide phase in the sample produced at 700°C is much lower: 69.1%. The situation is most interesting for the sample obtained by the carbonization at 1000°C: the content of the phase (Ta,Hf)C in it approaches that in the first sample and is 85.4%. However, because the initial powder after the carbonization contains already no less than 19–20% tantalum hafnium carbide, the increase in its content during dynamic heating to 1400°C is only ~65–66%.

CONCLUSIONS

In this work, the new method was developed to produce the finely divided and chemically active material Ta_2O_5–HfO_2–C, which is promising for reactive hot pressing or spark plasma sintering of ceramics based on complex tantalum hafnium carbide.

The method includes the simultaneous initiation of the hydrolysis of tantalum–hafnium-containing precursors of the class of alkoxides and alkoxoacetylacetonates of metals and the acid-catalyzed polymerization of furfuryl alcohol to form a dense gel (procedure for creating interpenetrating organic–inorganic networks). The concentration ranges were determined within which one can avoid the uncontrollable hydrolysis or polymerization preventing the formation of connected-disperse systems.

The samples of the Ta_2O_5–HfO_2–C system with different reactivities in the carbothermal synthesis of complex carbides were obtained based on the xerogel produced after drying using carbonization under dynamic vacuum conditions at various temperatures (400, 700, and 1000°C). Their elemental and phase composition, microstructure and thermal behavior in an air flow were studied. It was noted that, owing to the high carbonization temperature (1000°C), already this reaction step can give ≥19–20% nanocrystalline carbide phase, the oxidation of which in air begins at a temperature as low as ~220°C. Conversely, the sample synthesized at the minimum temperature 400°C has quite a high content of unpyrolyzed organic fragments (to 3–4 wt %).

The analysis of the thermal behavior of the obtained systems Ta_2O_5–HfO_2–C during heating to 1400°C in an inert gas flow showed that, as it was expected, the maximum reactivity (maximum content of the tantalum hafnium carbide synthesized in this process) was characteristic of the sample with the minimum carbonization temperature. However, in the case of using it for the reactive high-temperature consolidation of carbide ceramics, one should take into account the active gas release early in the pressing, which may break the vacuum in the chamber.

The minimum reactivity in the carbothermal synthesis in an argon flow was demonstrated by the system Ta_2O_5–HfO_2–C–(Ta,Hf)C produced by the carbonization of the xerogel at the highest temperature 1000°C. Although the final content of the carbide phase is high (~85%) and there are no residual organic fragments, this system is hardly worth using for reactive hot pressing or spark plasma sintering because the heating leads to the crystallization of not only tantalum oxide, but also much less reactive hafnium oxide.

The obtained data makes it possible to consciously choose the carbonization temperature of tantalum–hafnium–polymer-containing xerogels to form the maximum reactive Ta_2O_5–HfO_2–C materials for subsequent production of carbide ceramics in the TaC–HfC system.

ACKNOWLEDGMENTS

The microstructure and phase composition of the samples were studied using equipment of the Center for Shared Use of Physical Investigation Methods, Kurnakov Institute of General and Inorganic Chemistry, Russian Academy of Sciences, Moscow, Russia, which functions under a state assignment for basic scientific research for the Kurnakov Institute of General and Inorganic Chemistry.

FUNDING

This work was supported by the Russian Foundation for Basic Research (project no. 20-03-00502).

CONFLICT OF INTEREST

The authors declare that they have no conflicts of interest.

REFERENCES

1. G. V. Samsonov, *Refractory Transition Metal Compounds* (Academic, New York, 1964).
2. E. Rudy, F. Benesovsky, and L. E. Toth, Z. Metallkd. **54**, 345 (1963).
3. H. Nowotny, R. Kieffer, F. Benesovsky, et al., Monatsh. Chem. **90**, 669 (1959).
4. C. Agte and H. Alterthum, Z. Tech. Phys. **6**, 182 (1930).
5. D. L. Deadmore, J. Am. Ceram. Soc. **48** (7), 357 (1965).
6. R. A. Andrievskii, N. S. Strel'nikova, N. I. Poltoratskii, et al., Powder Metall. Met. Ceram. **6**, 65 (1967). https://doi.org/10.1007/BF00773385
7. I. G. Barantseva, V. N. Paderno, and Y. B. Paderno, Powder Metall. Met. Ceram. **6**, 139 (1967).
8. E. Rudy and H. Nowotny, Monatsh. Chem. **94**, 507 (1963). https://doi.org/10.1007/BF00903490
9. V. V. Fesenko and A. S. Bolgar, *Evaporation of Refractory Compounds* (Metallurgiya, Moscow, 1966) [in Russian].
10. R. Kieffer and F. Benesowsky, *Hartstoffe* (Springer, Wien, 1963).
11. H. Holleck, *Binäre und Ternäre Carbid-und Nitridsysteme der Übergangsmetalle* (Bornträger, Berlin, 1984).
12. E. Rudy, H. Nowotny, F. Benesovsky, et al., Monatsh. Chem. **91**, 176 (1960). https://doi.org/10.1007/BF00903181
13. H. Nowotny, R. Kieffer, F. Benesovsky, et al., Monatsh. Chem. **90**, 669 (1959). https://doi.org/10.1007/BF00902392
14. H. Bittner and H. Goretzki, Monatsh. Chem. **91**, 616 (1960). https://doi.org/10.1007/BF00899797
15. O. Cedillos-Barraza, D. Manara, K. Boboridis, et al., Sci. Rep. **6**, 37962 (2016). https://doi.org/10.1038/srep37962
16. A. I. Savvatimskiy, S. V. Onufriev, and S. A. Muboyadzhyan, J. Eur. Ceram. Soc. **39**, 907 (2019). https://doi.org/10.1016/j.jeurceramsoc.2018.11.030
17. C. Zhang, A. Gupta, S. Seal, et al., J. Am. Ceram. Soc. **100**, 1853 (2017). https://doi.org/10.1111/jace.14778
18. C. Zhang, B. Boesl, and A. Agarwal, Ceram. Int. **43**, 14798 (2017). https://doi.org/10.1016/j.ceramint.2017.07.227
19. L. Feng, J.-M. Kim, S.-H. Lee, et al., J. Am. Ceram. Soc. **99**, 1129 (2016). https://doi.org/10.1111/jace.14144
20. V. Shahedifar and M. G. Kakroudi, Int. J. Refract. Met. Hard Mater. **71**, 15 (2018). https://doi.org/10.1016/j.ijrmhm.2017.10.025
21. E. P. Simonenko, N. P. Simonenko, V. G. Sevastyanov, et al., Russ. J. Inorg. Chem. **64**, 1697 (2019). https://doi.org/10.1134/S0036023619140079

22. E. P. Simonenko, N. P. Simonenko, V. G. Sevast'yanov, et al., *Ultra-High-Temperature Ceramic Materials: Modern Problems and Trends* (IP A. V. Konyakhin, Ryazan', 2020) [in Russian].
23. E. P. Simonenko, N. P. Simonenko, A. N. Gordeev, et al., J. Eur. Ceram. Soc. **41**, 1088 (2021). https://doi.org/10.1016/j.jeurceramsoc.2020.10.001
24. E. P. Simonenko, N. P. Simonenko, A. S. Lysenkov, et al., Russ. J. Inorg. Chem. **65**, 446 (2020). https://doi.org/10.1134/S0036023620030146
25. H.-L. Liu, J.-X. Liu, H.-T. Liu, et al., Scr. Mater. **107**, 140 (2015). https://doi.org/10.1016/j.scriptamat.2015.06.005
26. M. Xiang, J. Gu, W. Ji, et al., Ceram. Int. **44**, 8417 (2018). https://doi.org/10.1016/j.ceramint.2018.02.035
27. M. G. Kakroudi, M. D. Alvari, M. Sh. Asl, et al., Ceram. Int. **46**, 3725 (2020). https://doi.org/10.1016/j.ceramint.2019.10.093
28. E. P. Simonenko, N. P. Simonenko, E. K. Papynov, et al., J. Sol-Gel Sci. Technol. **82**, 748 (2017). https://doi.org/10.1007/s10971-017-4367-2
29. E. P. Simonenko, N. P. Simonenko, E. K. Papynov, et al., Russ. J. Inorg. Chem. **63**, 1 (2018). https://doi.org/10.1134/S0036023618010187
30. E. P. Simonenko, N. P. Simonenko, A. N. Gordeev, et al., J. Sol-Gel Sci. Technol. **92**, 386 (2019). https://doi.org/10.1007/s10971-019-05029-9
31. E. P. Simonenko, N. P. Simonenko, A. S. Mokrushin, et al., Russ. J. Inorg. Chem. **64**, 1849 (2019). https://doi.org/10.1134/S0036023619140109
32. V. G. Sevastyanov, E. P. Simonenko, N. A. Ignatov, et al., Russ. J. Inorg. Chem. **56**, 661 (2011). https://doi.org/10.1134/S0036023611050214
33. E. P. Simonenko, N. A. Ignatov, N. P. Simonenko, et al., Russ. J. Inorg. Chem. **56**, 1681 (2011). https://doi.org/10.1134/S0036023611110258
34. E. P. Simonenko, N. P. Simonenko, A. V. Derbenev, et al., Russ. J. Inorg. Chem. **58**, 1143 (2013). https://doi.org/10.1134/S0036023613100215
35. E. P. Simonenko, N. P. Simonenko, M. I. Petrichko, et al., Russ. J. Inorg. Chem. **64**, 1317 (2019). https://doi.org/10.1134/S0036023619110196
36. F. Li, J. Liu, X. Huang, et al., J. Am. Ceram. Soc. **102**, 5746 (2019). https://doi.org/10.1111/jace.16488
37. X.-F. Zhang, Z. Chen, Y. Feng, et al., ACS Sustain. Chem. Eng. **6**, 1068 (2018). https://doi.org/10.1021/acssuschemeng.7b03375
38. Y. Miao, Z. Yang, J. Rao, et al., Ceram. Int. **43**, 4372 (2017). https://doi.org/10.1016/j.ceramint.2016.12.083
39. M. S. Chandrasekar and N. R. Srinivasan, Ceram. Int. **42**, 8900 (2016). https://doi.org/10.1016/j.ceramint.2016.02.145
40. Y. Kong, Y. Zhong, X. Shen, et al., Mater. Lett. **99**, 108 (2013). https://doi.org/10.1016/j.matlet.2013.02.047
41. Y. Kong, Y. Zhong, X. Shen, et al., J. Porous Mater. **20**, 845 (2013). https://doi.org/10.1007/s10934-012-9660–4
42. Y. Badhe and K. Balasubramanian, RSC Adv. **4**, 28956 (2014). https://doi.org/10.1039/C4RA03316G
43. B. Liu, W. Ju, J. Zhang, et al., J. Sol-Gel Sci. Technol. **83**, 100 (2017). https://doi.org/10.1007/s10971-017-4400–5
44. D. H. Wang and X. Fu, Adv. Mater. Res. **194–196**, 562 (2011). https://doi.org/10.4028/www.scientific.net/AMR.194-196.562
45. B. S. Mojarad, A. Nourbakhsh, R. E. Kahrizsangi, et al., Ceram. Int. **41**, 5287 (2015). https://doi.org/10.1016/j.ceramint.2014.12.007
46. Y. Zhang, Z. Yuan, and Y. Zhou, Ceram. Int. **40**, 7873 (2014). https://doi.org/10.1016/j.ceramint.2013.12.134
47. M. Zhou, P. D. D. Rodrigo, X. Wang, et al., J. Eur. Ceram. Soc. **34**, 1949 (2014). https://doi.org/10.1016/j.jeurceramsoc.2014.01.028
48. X. Wang, M. Lu, L. Qiu, et al., Ceram. Int. **42**, 122 (2016). https://doi.org/10.1016/j.ceramint.2015.08.017
49. J. Zhong, Y. Peng, M. Zhou, et al., Microporous Mesoporous Mater. **190**, 309 (2014). https://doi.org/10.1016/j.micromeso.2014.02.029
50. J. Zhong, S. Liang, J. Zhao, et al., J. Eur. Ceram. Soc. **32**, 3407 (2012). https://doi.org/10.1016/j.jeurceramsoc.2012.04.047
51. C. Ang, A. Seeber, T. Williams, et al., J. Eur. Ceram. Soc. **34**, 2875 (2014). https://doi.org/10.1016/j.jeurceramsoc.2014.04.015
52. F. Li and X. Huang, J. Eur. Ceram. Soc. **38**, 1103 (2018). https://doi.org/10.1016/j.jeurceramsoc.2017.11.031
53. V. G. Sevast'yanov, E. P. Simonenko, N. P. Simonenko, et al., Russ. J. Inorg. Chem. **57**, 307 (2012). https://doi.org/10.1134/S0036023612030278
54. E. P. Simonenko, N. P. Simonenko, Y. S. Ezhov, et al., Phys. At. Nucl. **78**, 1357 (2015). https://doi.org/10.1134/S106377881512011X
55. L. A. Aleshina and S. V. Loginova, Crystallogr. Rep. **47**, 415 (2002). https://doi.org/10.1134/1.1481927
56. T. F. Fedorov, *Carbon–Hafnium-Tantalum Ternary Alloy Phase Diagram 1000°C* (ASM Alloy Phase Diagrams Center, Materials Park, OH, 2007).
57. A. I. Gusev, Zh. Fiz. Khim. **59**, 579 (1985).
58. M. von Schwarz and O. Summa, Met. Met. Met. **12**, 298 (1933).
59. O. Ohtaka, T. Yamanaka, and S. Kume, J. Ceram. Soc. Jpn. **99**, 826 (1991). https://doi.org/10.2109/jcersj.99.826
60. N. C. Stephenson and R. S. Roth, Acta Crystallogr., Sect. B: Struct. Crystallogr. Cryst. Chem. **27**, 1037 (1971). https://doi.org/10.1107/S056774087100342X

Translated by V. Glyanchenko